



Effect of ground state charge transfer and photoinduced charge separation on the energy level alignment at metal halide perovskite/organic charge transport layer interfaces

Lennart Frohloff¹ · Fengshuo Zu¹ · Dongguen Shin¹ · Norbert Koch^{1,2}

Received: 11 October 2022 / Accepted: 10 March 2023 / Published online: 21 March 2023
© The Author(s) 2023

Abstract

One of the most promising routes for the future fabrication of solution-processable high-performance solar cells is to employ metal halide perovskites as photoactive material combined with organic semiconductors as charge extraction layers. An essential requirement to obtain high device performance is a proper energy level alignment across the device interfaces. Here, we investigate the interface between a triple cation perovskite and a prototypical electron acceptor molecule. Photoemission spectroscopy reveals a ground state charge transfer induced band bending on either side of the junction, which significantly alters the charge extraction barriers as compared to assumed vacuum level alignment and flat-band conditions. In addition, we demonstrate that upon white light illumination, the energy levels of the organic layer exhibit rigid shifts by up to 0.26 eV with respect to those of the perovskite, revealing a non-constant energy offset between the frontier energy levels of the two materials. Such level shifts of the organic transport layer are fully reversible upon switching on/off the light, indicating an electrostatic origin of this phenomenon caused by unbalanced distribution of photogenerated charge carriers. We therefore stress the importance of determining the energy level alignment at perovskite-based interfaces not only in the electronic ground state (dark) but also under device operating conditions (*operando*) to enable for a reliable correlation with the device performance.

Keywords Energy level alignment · Photoelectron spectroscopy · Metal halide perovskites · Organic semiconductors

1 Introduction

A thorough understanding of the energy level alignment at semiconductor junctions is of paramount importance for efficient operation of optoelectronic devices, but it is presently not comprehensively available for metal halide perovskite-based interfaces [1–5]. In the realm of perovskite photovoltaics, where the charge extraction layers are often made of organic semiconductors, a tailored design of energy levels ensures selective transport of charge carriers and enables a low interfacial recombination probability of electrons and holes in the device. Low recombination losses and efficient

spatial carrier separation generally go hand-in-hand with a high open-circuit voltage, short-circuit current, as well as fill factor, and therefore, high power conversion efficiency of the solar cells [6, 7]. Estimating the energy level alignment of perovskite/organic semiconductor heterojunctions a priori is, however, not straightforward. Effects like band bending [8–10], the order of deposition [11], and/or the orientation of the organic molecules [12] may cause the actual interface to deviate considerably from estimates made with the assumption of a constant vacuum level across the interface with energy levels determined for the separate materials [13].

In addition, it was long accepted knowledge that the interfacial energy level offset would be fixed upon establishment of the interface between two materials in direct contact. However, recent studies demonstrated that the interfacial energy levels experience a realignment upon photoexcitation of junctions comprising lead halide perovskites [14]. Such a realignment under illumination, i.e. change of energy offsets for charge extraction and transport, was attributed to the accumulation of one type of charge carriers in the organic

✉ Norbert Koch
norbert.koch@physik.hu-berlin.de

¹ Institut für Physik & IRIS Adlershof, Humboldt-Universität zu Berlin, 12489 Berlin, Germany

² Helmholtz-Zentrum Berlin für Materialien und Energie GmbH, 12489 Berlin, Germany

transport or perovskite layer at the interface, favored by the weak electronic coupling between the materials. Although clear evidence of the energy level realignment upon illumination was demonstrated for a few cases [14], the level alignment at the electron transport layer/perovskite junction in the electronic ground state (in dark) has not yet been investigated in sufficient detail.

Here, we present a comprehensive ultraviolet and X-ray photoelectron spectroscopy (UPS and XPS) study of the energy level alignment of a prototypical organic electron acceptor semiconductor (perylene-tetracarboxylic dianhydride, abbreviated as PTCDA) in contact with a modern triple cation perovskite (with the cations Cs, formamidinium, and methylammonium, abbreviated as CsFAMA). We reveal a pronounced ground state electron transfer from the perovskite to the acceptor molecules, leading to the build-up of a space-charge region upon forming the interface. As a consequence, a band bending of 0.40 eV was observed in the perovskite near-interface region, accompanied by electron accumulation in the acceptor molecular layer close to the interface. Due to the presence of these excess electrons, the lowest unoccupied molecular orbital (LUMO) level of the formerly neutral acceptor molecules was found to split into an upper unoccupied and a lower singly occupied molecular orbital (SOMO) level by Coulomb repulsion [15], where the intensity- and energy-evolution of the SOMO as well as the relaxed HOMO of the anions as a function of film thickness were revealed by UPS. Additional white light illumination during UPS measurements provides further evidence for the previously proposed energy level realignment mechanism that rigidly shifts the energy levels of the organic layer while leaving the energy levels of the perovskite essentially unchanged.

2 Experimental details

2.1 Sample fabrication

The ITO substrates were cleaned with detergent, deionized water, acetone and isopropanol subsequently for 10 min in an ultrasonic bath each. Next, they were UV-ozone treated for 10 min. The cleaned substrates were then introduced into a Nitrogen-filled glovebox (O_2 , H_2O content < 0.5 ppm), where all perovskite films were deposited. For the triple-cation perovskite precursor, three individual precursors were prepared, namely a formamidinium lead iodide (FAPbI₃) solution, a methylammonium lead bromide (MAPbBr₃) solution and a CsI solution. Both perovskite solutions were prepared from nominal 1.0 M solutions with a lead salt excess of 9 mol%. In details, for the FAPbI₃ solution, 201.0 mg PbI₂ (Tokyo Chemical Industry, 99.99% purity on trace metals basis, $> 98.0\%$ total purity) and 68.8 mg FAI

(GreatCellSolar, 99.99% purity) were dissolved in 320 μ l N,N-dimethylformamide (DMF, Sigma-Aldrich, 99.8% purity, anhydrous) and 80 μ l dimethyl sulfoxide (DMSO, Sigma-Aldrich, $\geq 99.9\%$ purity, anhydrous). The MAPbBr₃ precursor consisted of 80.0 mg PbBr₂ (TCI, $> 98.0\%$ total purity) and 22.4 mg MABr (GreatCellSolar, 99.99% purity) dissolved in 160 μ l DMF and 40 μ l DMSO. 77.9 mg CsI (Sigma-Aldrich, 99.999% purity on trace metals basis) were dissolved in 200 μ l DMSO (= 1.5 M). After stirring for several hours, the FAPbI₃ and MAPbBr₃ solutions were mixed in a volume ratio of 83:17, before adding 5 vol.% of the CsI solution to obtain the CsFAMA precursor. 22.8 mg thiourea (TU, TCI, $> 99.0\%$ purity) were dissolved in 200 μ l DMF (= 1.5 M) and added to the pre-mixed CsFAMA precursor in a concentration of 15 vol.%. All solutions, apart from the CsI, were prepared freshly and not used for longer than two days.

The CsFAMA precursor was spin-coated onto the ITO substrates at 3500 rpm for 35 s. 150 μ l of the anti-solvent anisole (Sigma-Aldrich, 99.7% purity, anhydrous) were dripped onto the sample 15 s after the spin start. Immediately afterwards, the samples were annealed on a 100 °C hot plate for 15 min. The CsFAMA samples were introduced into the ultra-high vacuum (UHV) system for PES measurements without exposure to ambient air. The PTCDA (Sigma-Aldrich, 97% purity) was deposited from a heated quartz crucible in the preparation chamber of the PES system. The material was introduced into the UHV system as-received and thoroughly degassed for several hours before deposition. The nominal thickness of PTCDA was directly measured by a quartz crystal microbalance.

2.2 Photoemission measurements

The photoemission spectra were recorded using a hemispherical electron analyzer (SPECS Phoibos 100) in a UHV system equipped with a monochromated He I ($h\nu = 21.218$ eV) source for UPS and a standard Mg K α ($h\nu = 1253.6$ eV, anode power = 30 W) X-ray source for XPS. The base pressure of the analysis chamber was 1×10^{-9} mbar. All spectra were recorded at room temperature and under normal emission. For measurement of the SECO, a sample bias of -10.0 V was applied to overcome the analyzer work function. A Solux MR16 4700 K white halogen lamp (intensity equivalent to 150 mW/cm²) was employed for illumination.

2.3 Atomic force microscopy measurements

The atomic force microscopy experiments were conducted in a Bruker Dimension FastScan under ambient air in ScanAsyst Air mode.

3 Results and discussion

The triple-cation perovskite $\text{Cs}_{0.05}[\text{FA}_{0.83}\text{MA}_{0.17}]_{0.95}\text{Pb}[\text{I}_{0.83}\text{Br}_{0.17}]_3$ (CsFAMA) was chosen as the photoactive material because of its long-term stability and high performance in photovoltaics [16]. As shown by Patil et al. [17], adding a small amount of thiourea (TU) into the perovskite precursor can massively increase the size of the crystallites in the thin film. Therefore, 15 vol.% of a 1.5 M TU solution were added to the perovskite precursor prior to spin-coating onto indium tin oxide (ITO) substrates. These large-grain perovskite thin films are, besides their reported superior photovoltaic characteristics, of fundamental interest as they provide atomically flat grain facets on the scale of several μm^2 , which is ideal for a homogenous growth of the thermally deposited acceptor molecules. The organic molecule perylene-3,4,9,10-tetracarboxylic dianhydride (PTCDA)

was selected as a strong electron acceptor that exhibits high stability in ultra-high vacuum and under 1.5 suns illumination.

3.1 Energy level alignment at the PTCDA/perovskite interface in the electronic ground state

To establish the band alignment at the PTCDA/CsFAMA interface, the PTCDA molecules were thermally deposited in a step-by-step manner on top of a CsFAMA on ITO substrate. UPS measurements were performed in situ after each deposition increment. Figure 1a, b show the secondary electron cut-off (SECO) and valence spectra as functions of the PTCDA layer thickness, respectively. The pristine CsFAMA thin film on ITO exhibits a work function of 4.15 eV and a valence band (VB) onset at 1.20 eV binding energy (BE) with respect to the Fermi level (set to 0 eV BE). The extrapolation of the VB onset was performed by plotting the photoelectron intensity on a logarithmic intensity scale,

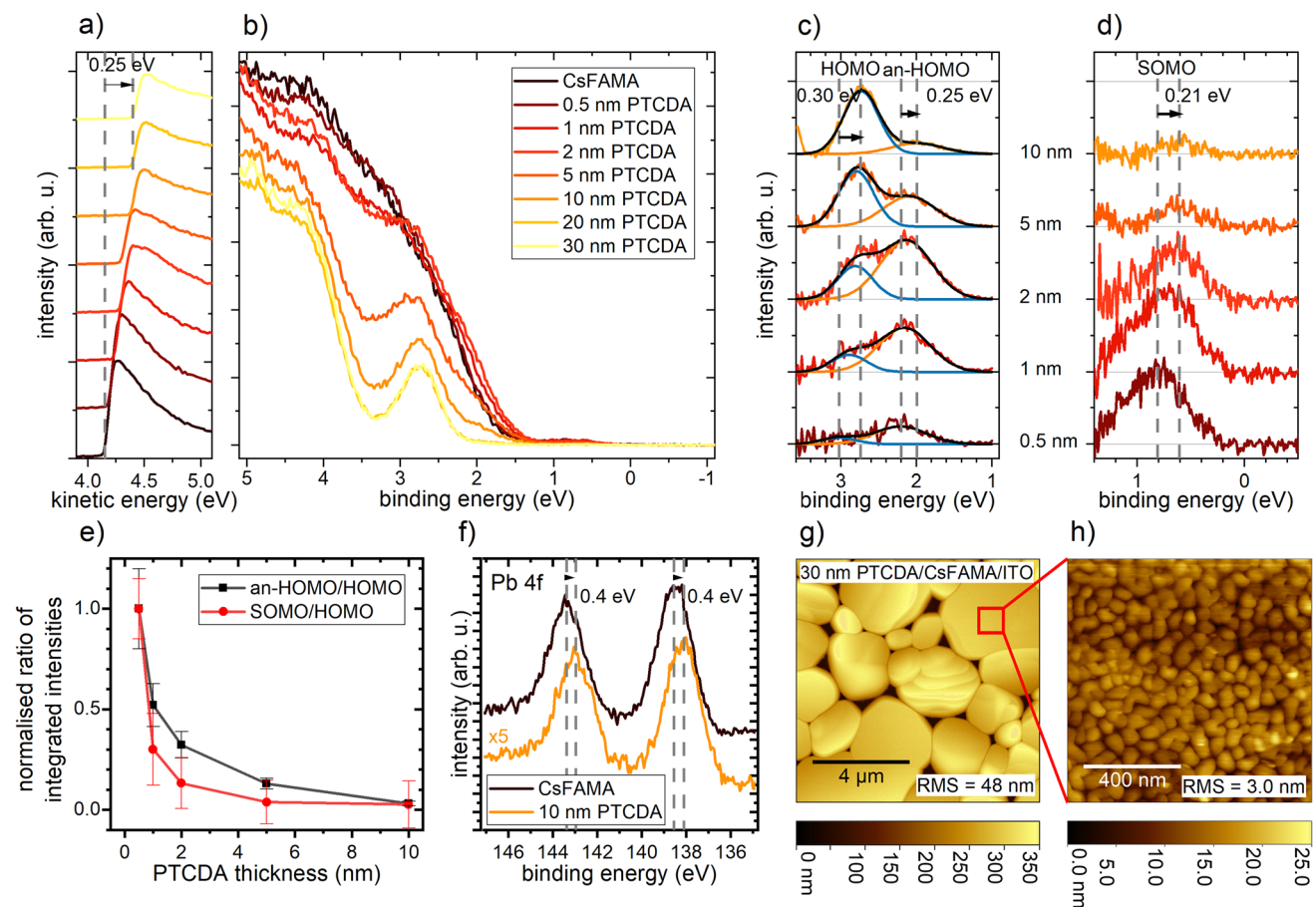


Fig. 1 The **a** secondary electron cut-off (SECO) and **b** valence band (VB) spectra of the PTCDA/CsFAMA interface with incrementally increased PTCDA thickness. **c** Background-subtracted PTCDA HOMO (blue line) and anion HOMO regions (an-HOMO, orange line) and **d**) PTCDA SOMO region by subtracting appropriately

scaled CsFAMA backgrounds. **e** The ratio of an-HOMO/HOMO and SOMO/HOMO intensities as a function of PTCDA thickness. **f** The XPS spectra of the Pb 4f core levels before and after 10 nm PTCDA deposition. **g**, **h** The AFM topography images of CsFAMA/ 30 nm PTCDA sample

which is commonly applied to accurately infer the band edge positions for metal halide perovskites [18, 19]. Upon increasing the PTCDA layer thickness, the work function increases gradually from 4.15 eV and saturates at 4.40 eV for a nominally 20 nm thick PTCDA layer. Concomitantly, the valence band shape exhibits a gradual transition from the typical CsFAMA features to PTCDA-only features [20]. Further PTCDA deposition up to 30 nm was found to leave the work function and valence features unchanged.

In more detail, with increasing thickness of the PTCDA layer a clearly visible peak in the region around 2.8 eV BE emerges. It becomes clearly discernible for nominal thicknesses larger than 5 nm and can be attributed to the highest occupied molecular orbital (HOMO) level of PTCDA. For a better visualization of the evolution of PTCDA HOMO features, the top VB region is rescaled by subtracting the background of the CsFAMA valence bands, as presented in Fig. 1c, d. Further information on the fitting procedure can be found in the Supplementary Information.

As displayed in Fig. 1c, we observed the emergence of a distinct second peak at the lower BE side of ca. 2.2 eV at a sub-monolayer PTCDA. Its BE position and intensity experience noticeable changes upon increasing the PTCDA thickness. We thus assign this peak to the HOMO of negatively charged PTCDA anions (denoted as an-HOMO) due to electron transfer required to reach electronic equilibrium throughout the heterojunction. The HOMO and an-HOMO shift to lower BE upon increasing the PTCDA thickness by 0.30 eV and 0.25 eV, respectively, in line with the measured SECO shift and thus demonstrates downward band bending towards the interface within the PTCDA layer. The absolute intensity of the an-HOMO peak increases with PTCDA thickness up to 2 nm and then starts to decrease until it becomes too low to be detected for PTCDA thicknesses greater than 10 nm. This dependence indicates the localization of charged PTCDA anions at the interface. The relation between the an-HOMO/HOMO intensity ratio and the film thickness, as presented in Fig. 1e, is directly proportional to the fraction of charged PTCDA molecules. It illustrates an integer ground state charge transfer process between the CsFAMA and the PTCDA molecules, i.e., a fraction of PTCDA molecules receive an integer negative charge [15, 21]. The fact that the charged molecules seem to persist for thicknesses up to 10 nm is likely due to the island-growth mode of PTCDA molecules, preventing a fast formation of a fully-closed layer of PTCDA, as shown in Fig. 1h.

Due to the electron transfer from CsFAMA to the PTCDA molecules, the LUMO levels of the formerly neutral acceptor molecules are split into an upper singly unoccupied level and a lower SOMO level by Coulomb repulsion. The evolution of the SOMO as a function of PTCDA layer thickness is presented in Fig. 1d. For the SOMO levels, a shift of ca. 0.21 eV to lower BE can be observed, in line with the shift

of the SECO and HOMO levels. As the an-HOMO and the SOMO both originate from the PTCDA anions, their relative intensities over that of the neutral HOMO are found to follow the same trend with increasing PTCDA thickness, as shown in Fig. 1e. Regarding the band alignment in the perovskite layer, the interfacial charge transfer leads to an upward band bending by 0.40 eV towards the interface in the perovskite, as evidenced by the shifts of the Pb 4f peaks to lower BE in Fig. 1f. This upward band bending is consistent with the accumulation of a positive space-charge on the CsFAMA side of the heterojunction.

Based on these photoemission data, the energy level alignment at the PTCDA/CsFAMA interface in the ground state (dark) can be established, as displayed in Fig. 2a. The pristine CsFAMA surface appears as a n-type semiconductor with the Fermi level positioned rather close to the conduction band minimum. The n-type surface is assumed to represent the bulk properties, given that no surface photovoltage was observed upon additional white light illumination, indicating the absence of surface states (see Fig. S2) [23]. It is noted that the vacuum level shift of more than 0.5 eV at the CsFAMA/ITO interface is likely linked to the occurrence of an interface dipole and/or band bending [24].

3.2 Energy level realignment of the PTCDA/CsFAMA interface under illumination

Now that the exact energy level alignment at the PTCDA/CsFAMA interface in the electronic ground state is determined, the level alignment closer to device operation conditions, i.e. under illumination, is further examined. In order to assure the reproducibility of the results, a fresh sample was used for these experiments. We found essentially the same band alignment at the PTCDA/CsFAMA interface, which again exhibits a type-II junction. However, the CsFAMA exhibits initially a slightly stronger n-type character with its CBM positioned at 0.27 eV above the Fermi level, which is within the typical sample-dependent variation often observed for metal halide perovskites.

Under white light illumination equivalent to ca. 1.5 suns during the UPS measurements, we observed a rigid shift of the PTCDA energy levels [surface electrostatic potential (SEP) and valence levels] to lower BE by 0.26 eV, as shown in Fig. 3. Here, the SEP denotes the "work function under illumination", nevertheless, both refer to the energy difference between the vacuum level and the Fermi level of the conductive ITO substrate. Such shift is found to be reversible once switching off the light, thus manifesting an electrostatic origin. As revealed by recent studies [14, 24], the observed realignment of PTCDA energy levels is attributed to a photoinduced space-charge accumulation in the organic layer, which is driven by the large energy offset for electron extraction at the PTCDA/CsFAMA interface. The

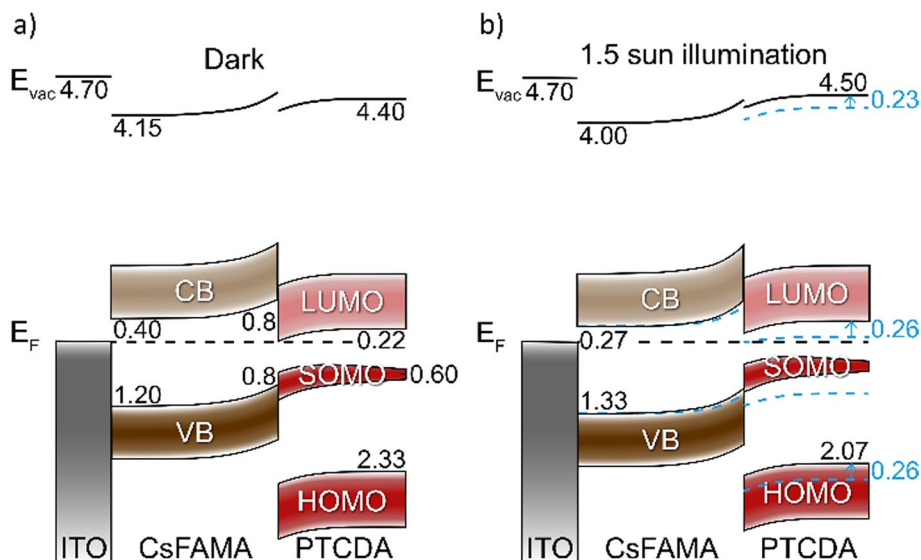


Fig. 2 Energy level diagram of the PTCDA/CsFAMA/ITO system determined **a** in dark and **b** under white light illumination. The position of the CsFAMA conduction band (CB) minimum and PTCDA LUMO were calculated by considering the band gaps of 1.60 eV (see Fig. S1) and 2.55 eV [22], respectively. The slight deviations

of the perovskite energy levels between **a**, **b** originate from sample-to-sample variations, where the illumination experiments in **b**) were performed on a fresh PTCDA/CsFAMA sample. E_{vac} and E_F refer to vacuum level and Fermi level (at 0 eV BE), respectively. The dashed blue lines indicate the band onset positions of the sample in dark

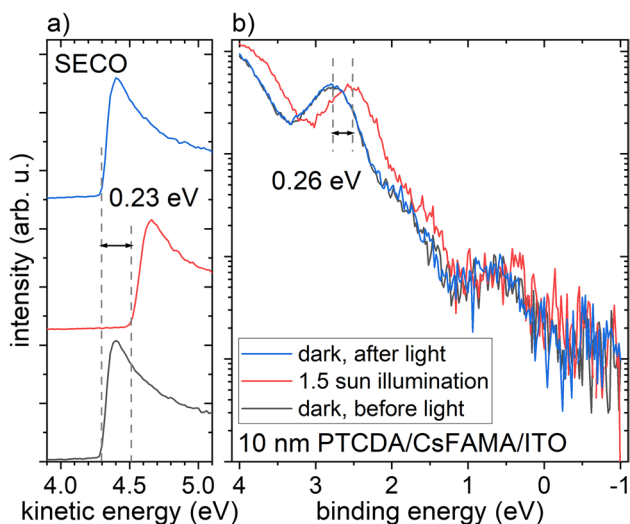


Fig. 3 UPS spectra of the PTCDA/CsFAMA/ITO stack measured in dark and under white light illumination. Reversible shifts of the **a** SECO and **b** HOMO levels of the PTCDA layer

photoactive material CsFAMA generates free charge carriers under illumination of which the electrons are efficiently transferred into the PTCDA layer. The realignment due to charge accumulation is expected to take place already at the very interface on the scale of monolayer length [14].

The accumulation of mobile electronic charges at perovskite/charge transport layer interfaces under illumination has been suggested earlier from illumination-dependent

capacitance changes [25]. In analogy to the modelling performed in Ref. [24], the amount of charge accumulated in the present case amounts to ca. 10^{17} cm^{-3} , similar in magnitude to the findings in Ref. [25]. It should be noted that also ionic charge can accumulate at such interfaces due to ion movement [26, 27], however, on slower time scales compared to the electronic charge accumulation discussed here.

We would like to note that a band flattening, i.e. the surface photovoltage (SPV) effect, and a consequential shift of the PTCDA energy levels can be ruled out, as the SPV effect would lead to a downward shift of the PTCDA energy levels, in opposite direction to our experimental observations. The perovskite energy levels remain essentially constant under illumination, as demonstrated from the Pb 4f core levels (see Fig. S3).

A similar realignment phenomenon of the perovskite/organic semiconductor interfaces was also observed employing the commonly used C_{60} molecular electron transport layer, where the C_{60} energy levels exhibit rigid upward shifts by ca. 0.25 eV upon photoexcitation, illustrating a universal charge carrier-driven energy level realignment effect at perovskite-based type-II junctions. Details of the electronic structure at the C_{60} /CsFAMA interface are displayed in Fig. S4-S7 in the Supplementary Information.

4 Conclusion

We first established the band alignment at the PTCDA/CsFAMA interface in the electronic ground state, which exhibits a type-II heterojunction with a build-up of a space-charge region at the interface due to charge transfer. As a consequence, LUMO levels of the formerly neutral PTCDA molecules were found to split into an upper unoccupied level and a lower SOMO level by Coulomb repulsion, where the signatures of the SOMO and an-HOMO were clearly revealed by UPS. A detailed analysis further shows the presence of an upward band bending by 0.40 eV within the CsFAMA layer and a downward band bending by ca. 0.30 eV in the PTCDA layer towards the interface. The results highlight the importance of case-by-case studies by photoemission on perovskite-related interfaces as the simple vacuum level alignment assumption can lead to fatal deviations from its actual level alignment. Further UPS measurements under additional white light illumination demonstrate a realignment of the PTCDA energy levels relative to those of the perovskite, which leads to a variation in the energy offset between the frontier energy levels of the materials. These findings are in line with recent studies [14, 24] and underline the necessity of investigating the energy level alignment also under device operating conditions, i.e., *operando*, to enable reliable correlation with device functionality.

Supplementary Information The online version contains supplementary material available at <https://doi.org/10.1007/s00339-023-06564-7>.

Acknowledgements This work was funded by the Deutsche Forschungsgemeinschaft (DFG, German Research Foundation, Project numbers: 182087777-SFB951 and 423749265-SPP2196 “SURPRISE”).

Funding Open Access funding enabled and organized by Projekt DEAL.

Data availability Data are available from the corresponding author upon reasonable request.

Declarations

Conflict of interest The authors declare that there is no conflict of interest.

Open Access This article is licensed under a Creative Commons Attribution 4.0 International License, which permits use, sharing, adaptation, distribution and reproduction in any medium or format, as long as you give appropriate credit to the original author(s) and the source, provide a link to the Creative Commons licence, and indicate if changes were made. The images or other third party material in this article are included in the article's Creative Commons licence, unless indicated otherwise in a credit line to the material. If material is not included in the article's Creative Commons licence and your intended use is not permitted by statutory regulation or exceeds the permitted use, you will need to obtain permission directly from the copyright holder. To view a copy of this licence, visit <http://creativecommons.org/licenses/by/4.0/>.

References

1. S.M. Sze, K.K. Ng, *Physics of Semiconductor Devices*, 3rd edn. (Wiley, 2007)
2. N. Koch, *ChemPhysChem* **8**, 1438 (2007)
3. S. Braun, W.R. Salaneck, M. Fahlman, *Adv. Mater.* **21**, 1450 (2009)
4. N. Koch, *Appl. Phys. Lett.* **119**, 260501 (2021)
5. M. Fahlman, S. Fabiano, V. Gueskine, D. Simon, M. Berggren, X. Crispin, *Nat. Rev. Mater.* **4**, 627 (2019)
6. P. Schulz, *ACS Energy Lett.* **3**, 1287 (2018)
7. S.D. Stranks, *ACS Energy Lett.* **2**, 1515 (2017)
8. L. Kronik, Y. Shapira, *Surf. Sci. Rep.* **37**, 1 (1999)
9. H. Ishii, K. Sugiyama, E. Ito, K. Seki, *Adv. Mater.* **11**, 605 (1999)
10. M. Oehzelt, N. Koch, G. Heimel, *Nat. Commun.* **5**, 4174 (2014)
11. A. Kahn, N. Koch, W. Gao, *J. Polym. Sci. B Polym. Phys.* **41**, 2529 (2003)
12. S. Duhm, G. Heimel, I. Salzmänn, H. Glowatzki, R.L. Johnson, A. Vollmer, J.P. Rabe, N. Koch, *Nat. Mater.* **7**, 326 (2008)
13. H. Fukagawa, S. Kera, T. Kataoka, S. Hosoumi, Y. Watanabe, K. Kudo, N. Ueno, *Adv. Mater.* **19**, 665 (2007)
14. F. Zu, J.H. Warby, M. Stolterfoht, J. Li, D. Shin, E. Unger, N. Koch, *Phys. Rev. Lett.* **127**, 246401 (2021)
15. S. Winkler, P. Amsalem, J. Frisch, M. Oehzelt, G. Heimel, N. Koch, *Mater. Horiz.* **2**, 427 (2015)
16. M. Saliba, T. Matsui, J.Y. Seo, K. Domanski, J.P. Correa-Baena, M.K. Nazeeruddin, S.M. Zakeeruddin, W. Tress, A. Abate, A. Hagfeldt, M. Grätzel, *Energy Environ. Sci.* **9**, 1989 (2016)
17. J.V. Patil, S.S. Mali, C.K. Hong, *Nanoscale* **11**, 21824 (2019)
18. J. Endres, D.A. Egger, M. Kulbak, R.A. Kerner, L. Zhao, S.H. Silver, G. Hodes, B.P. Rand, D. Cahen, L. Kronik, A. Kahn, *J. Phys. Chem. Lett.* **7**, 2722 (2016)
19. F. Zu, P. Amsalem, D.A. Egger, R. Wang, C.M. Wolff, H. Fang, M.A. Loi, D. Neher, L. Kronik, S. Duhm, N. Koch, *J. Phys. Chem. Lett.* **10**, 601 (2019)
20. S. Park, N. Mutz, S.A. Kovalenko, T. Schultz, D. Shin, A. Aljarb, L.J. Li, V. Tung, P. Amsalem, E.J.W. List-Kratochvil, J. Stähler, X. Xu, S. Blumstengel, N. Koch, *Adv. Sci.* **8**, 1 (2021)
21. H. Wang, P. Amsalem, G. Heimel, I. Salzmänn, N. Koch, M. Oehzelt, *Adv. Mater.* **26**, 925 (2014)
22. K. Akaïke, K. Kanai, H. Yoshida, J. Tsutsumi, T. Nishi, N. Sato, Y. Ouchi, K. Seki, *J. Appl. Phys.* **104**, 023710 (2008)
23. F. Zu, C.M. Wolff, M. Ralaiarisoa, P. Amsalem, D. Neher, N. Koch, *A.C.S. Appl. Mater. Interfaces* **11**, 21578 (2019)
24. F. Zu, M. Roß, L. Frohloff, D. Shin, N. Tessler, S. Albrecht, N. Koch, *Solar RRL* **6**, 2101065 (2022)
25. I. Zarazua, J. Bisquert, G. Garcia-Belmonte, *J. Phys. Chem. Lett.* **7**, 525 (2016)
26. W. Tress, N. Marinova, T. Moehl, S.M. Zakeeruddin, M. Khaja Nazeeruddin, M. Grätzel, *Energy Environ. Sci.* **8**, 995 (2015)
27. G.A. Nemnes, C. Besleaga, A.G. Tomulescu, I. Pintilie, L. Pintilie, K. Torfason, A. Manolescu, *Sol. Energy Mater. Sol. Cells* **159**, 197 (2017)

Publisher's Note Springer Nature remains neutral with regard to jurisdictional claims in published maps and institutional affiliations.